# Author's Accepted Manuscript

Habitat characterization of the Vema Fracture Zone and Puerto Rico Trench

C.W. Devey, N. Augustin, A. Brandt, N. Brenke, J. Köhler, L. Lins, C. Schmidt, I.A. Yeo

**DEEP-SEA RESEARCH**
**PART II**

www.elsevier.com/locate/dsr2

Habitat characterization of the Vema Fracture Zone and Puerto Rico Trench

# C.W. Devey[a*], N. Augustin[a], A. Brandt[b, c, d], N. Brenke[e], J. Köhler[f], L. Lins[c,d,g,], C. Schmidt[a], I.A. Yeo[a,h]

[a]Geomar Helmholtz Institute for Ocean Research Kiel, Wischofstr. 1-3, D-24148 Kiel, Germany

[b]Zoological Museum Hamburg, Center of Natural History, University of Hamburg, Martin-Luther-King-Platz 3, D-20146 Hamburg, Germany

[c]Senckenberg Research Institute and Museum, Senckenberganlage 25, D-60325 Frankfurt, Germany (present address)

[d]Goethe-University of Frankfurt, FB 15, Institute for Ecology, Evolution and Diversity, Max-von-Laue-Str. 13, D-60439 Frankfurt am Main, Germany

[e]Deutsches Zentrum für Marine Biodiversitätsforschung (DZMB), Südstrand 44, D-26382 Wilhelmshaven, Germany

[f]Institute of Environmental Physics, University of Bremen, Otto-Hahn-Allee 1, D-28359 Bremen, Germany

[g]Marine Biology Department, Ghent University, Krijgslaan 281/S8, B-9000 Ghent, Belgium

[h]*Now at:* National Oceanography Centre, European Way, Southampton SO14 3ZH, U.K.

*Corresponding author. Tel.: +49 431 600 2257, ORCID-ID: 0000-0002-0930-7274. cdevey@geomar.de

## 1 Abstract

Although many of the regions on and close to the mid-ocean ridges have been extensively mapped and sampled, the abyssal intraplate regions remain essentially unsampled and unmapped, leaving huge gaps in our understanding of their geologic history and present activity. Prominent bathymetric features in these intraplate regions are fracture zones. Here we present bathymetric and sampling information from a transatlantic transect along the Vema Fracture Zone (ca. 11°N), covering crustal ages from 109 - 0Ma on the African plate and 0-62Ma on the South American plate. The Vema Fracture Zone is the intraplate trace of the active Vema Transform plate boundary, which offsets the present-day Mid-Atlantic Ridge by ca. 300 km left-laterally, juxtaposing zero-age crust with crust of 20 million years age. Our results show clear evidence of tectonic activity along most of the Fracture Zone, in most places likely associated with active fluid flow. Within the active Vema Transform at crustal ages of ca. 10Ma we found clear indications of fluid flow both in the sediments and the overlying water column. This region is >120 km from the nearest spreading axis and increases by almost an order of magnitude the maximum off-axis distance that active hydrothermal discharge has been found in the oceanic crust. Sampling of the igneous seafloor was possible at all crustal ages and the accretionary fabric imprinted on the plate during its production was prominent everywhere.

Seafloor sediments show signs of extensive bioturbation. In one area, high concentrations of spherical Mn-nodules were also found and sampled.

At the end of the transect we also mapped and sampled the Puerto Rico Trough, a >8000m deep basin north of the Caribbean arc. Here the seafloor morphology is more complicated and strongly influenced by transpressive tectonics.

## 2   Introduction

Despite the fact that they comprise over 50% of Earth´s surface, our knowledge of the deep ocean basins, how they were formed, what role they play in the Earth system on geological time scales and their influence on abyssal biogeography is rudimentary at best. Despite the name "abyssal plain", available data shows that they are generally not flat or featureless but are strongly influenced both by the underlying plate geology and subsequent sedimentary processes (e.g., Duin et al., 1984; Hensen et al., 2015; Mammerickx, 1970; Minshull et al., 2014; Pratt, 1965; Scholz et al., 2009).

One of the major classes of bathymetric features on the deep seafloor are fracture zones - off-axis traces of active first-order plate boundary offsets or transform faults (Macdonald and Fox, 1983; Wilson, 1965). Fracture zones extend in some cases for many hundreds of kilometers across the ocean basins, influencing basin-scale oceanography and ocean mixing (e.g., Clement et al., 2017; Ferron et al., 1998; Ledwell et al., 2000; Polzin et al., 1996; Polzin et al., 1997; Thurnherr et al., 2005), and possibly chemosynthetic biogeography (e.g., Mullineaux et al., 2002). Much of our knowledge of fracture zone locations comes from satellite altimetry work (e.g., Matthews et al., 2011; Muller and Roest, 1992) and few have been mapped acoustically in their entirety (a possible exception being Kane Fracture Zone, Tucholke and Schouten, 1989) . Although fracture zones are not part of the active plate boundary, they have been shown to be seismically active in some cases (McGuire and Beroza, 2012), although whether intraplate deformation is preferentially concentrated there is controversial (e.g., Bergman and Solomon, 1992). Subducting fracture zones have been shown to have a major effect on convergent margin seismicity (e.g., Dzierma et al., 2012; Lange et al., 2010; Nakajima and Hasegawa, 2006).

The Atlantic Ocean contains several large fracture zones, one of the most prominent being the Vema Fracture Zone. Several studies have been carried out on an uplifted ridge to the south of the younger regions of the Vema Fracture Zone (e.g., Bonatti et al., 2005; Cipriani et al., 2009) and the active plate boundary (the Vema Transform Fault) has also been extensively studied in terms of its deeper crustal structure (Detrick et al., 1982; Lagabrielle et al., 1992; Mamaloukasfrangoulis et al., 1991; Potts et al., 1986; Prince and Forsyth, 1988; van Andel et al., 1971) and lithologies (Cannat et al., 1991; Cannat and Seyler, 1995). Despite this, the Fracture Zone has remained unmapped and unsampled in its older regions both east and west of the Mid-Atlantic Ridge.

In December 2014/January 2015 we carried out an extensive multibeam mapping and sampling program during the maiden voyage of the new German Research Vessel "Sonne" along the whole extent of the Fracture Zone, including deep-submergence deployments of a mapping autonomous underwater vehicle.

The results, presented here, show it to be a structurally active region whose bathymetry records a long history of plate accretion.

Methods

## 2.1 Bathymetry

Bathymetric mapping was performed with the hull-mounted Kongsberg EM-122 system. This uses a nominal sound frequency of 12 kHz and up to 864 soundings per ping to generate depth soundings in up to 11 km of water. For the Vema Fracture Zone surveys, the beam spacing was set to be equiangle, meaning data were collected with approximately equal coverage on both port and starboard sides. Sound velocity profiles were extracted from the CTD on the AUV and/or the onboard CTD and were updated at every site. The majority of surveys were conducted with a symmetrical 1° beam spacing covering 60° to both sides of the vessel, a survey speed of 10 kn and a line spacing of 7 nm, giving a typical swath width on the seafloor of around 9 nm/17 km and yielding bathymetric grids with a final cell spacing of 60 m and no gaps. In the Puerto Rico Trench (PRT) greater water depths required a narrower beam width of 40° to both sides, yielding a similar typical swath width to earlier surveys of around 11 nm/20 km, the beam spacing was equidistant.

Post-processing and gridding of data was carried out using the DMagic and Fledermaus modules of the QPS Fledermaus software suite for 3D editing and gridding of the data. Multibeam data were cleaned manually to remove outliers and then gridded and imported to Global Mapper (Blue Marble). The final bathymetric maps presented in this work were produced using the texture shading technique (TTS) developed by Brown (2010) merged with minor weighted shaded relief and slope maps to remove any bias associated with the position of a light source. The final grid size of 60 m was chosen to provide the best overview while minimizing artifacts in the outer beams.

## 2.2 Autonomous Underwater Vehicle (AUV)

We deployed a 6000m-capable REMUS AUV (built by HYDROID Inc., Pocassett, USA) on seven missions within the Vema Fracture Zone. The vehicle has several possible configurations - during our deployments both the multibeam (which includes a Reson 7125 Seabat multibeam running at 200kHz) or camera (which includes a black-and-white camera and flash system and an Edgetech 2200-MP side-scan sonar running at 120kHz) configurations were used. During all deployments the AUV also collected environmental data using a Seabird SBE 49 FastCat CTD and an Eh sensor (the latter developed in collaboration with Dr. K. Nakamura, AIST Japan). The AUV navigation relative to the seafloor during individual dives was based on a Kearfott Inertial Navigation System coupled to a Teledyne RDI Workhorse navigator Doppler velocity logger operating at 300kHz. To place these AUV relative positions into the GPS latitude/longitude reference frame, we used the MB-System software package (Caress and Chayes, 1996) to achieve coincidence between the AUV measurements (bathymetric and side-scan features) and the ship-based bathymetry. The re-navigated multibeam data were processed and gridded using QINSy (QPS, Quality Positioning Services BV).

### 2.3  Sediment coring

Sediments were collected both with a 5m gravity corer (using a top weight of 1.3 - 1 tons) and a Multiple Corer (multicorer, MUC). The MUC is designed for sampling meiofauna (< 1mm) as well as sediments (Barnett et al., 1984), and employs 12 transparent acryl-glass-cylinders (tubes), each 62 cm in length. Each tube has an outer diameter of 99 mm, and an inner diameter of 94 mm, yielding a sampled surface area of 69.4 cm². Gravity corer samples were investigated for their pore water alkalinity on board the vessel. Analyses of total alkalinity (TA) were carried out using a METROHM Titration Unit SIS665. The TA was determined by titration with 0.2M HCl using a methyl red indicator. The titration vessel was bubbled with argon to strip any $CO_2$ or $H_2S$ during the titration. The IAPSO seawater standard was used to check the reproducibility and accuracy of the analyses.

### 2.4  Grain-size analysis

Multicorer cores were subjected to granulometry analyses using a Malvern Mastersizer 2000 with size range from 0.02 to 2000 µm. Each site had 2-3 replicate cores (for details of deployments see Table 1 and the individual site descriptions, below). Granulometry was calculated for one-centimeter intervals from the seafloor down to 5 cm depth. After being sliced, sample cores were frozen at -20 °C.

### 2.5  Camera-epibenthic sledge

The Camera-epibenthic sledge (C-EBS, Brandt et al., 2013) is equipped with a video camcorder (OKTOPUS; Sony HDR SR11E/SR12E) on the left side and a digital stills-camera (KONGSBERG; oe14-208/Canon G5) on the right side of the sledge. The cameras take videos and pictures from positions 0.8 m and 0.6 m above the sediment surface, respectively. At Sites 12 and 13 camera deployments were impossible because of water depth greater than 6000 m (maximum depth rating of the housings).

From the total of 8706 pictures recorded from all sites, only approx. 10% (883 images) were informative or useful, with sediment clouding often obscuring the view in the remaining pictures. From Sites 2 and 14, no images are available because of technical problems. Usable images are available from 8 EBS deployments (numbers indicate pictures from the still camera and camcorder, respectively): 4-9EBS (137/-), 6-8EBS (127/95), 8-4EBS (50/61), 9-2EBS (135/27), 9-8EBS (-/74), 11-1EBS (1/83), 11-4EBS (-/65), 14-1EBS (28/-).

## 3  Results and Discussion

Six sites along the Vema Transform/Fracture Zone and three sites in the Puerto Rico Trench were studied in detail. An overview of the relative positions of these sites together with the cruise track are shown in Figure 1. Figure 2 shows details of the bathymetry and gear deployed at the sites along the Vema Fracture Zone/Transform. General information on the stations occupied at all sites is presented in Table 1 and each station is assigned a lithospheric age based on the 6-minute-resolution age grid of Müller et al. (2008). Macrofaunal and

meiofaunal composition along the Vema Fracture Zone is described by Brandt et al. (present volume) and Schmidt et al. (present volume).

**Figure 1: Cruise track for the SO-237 voyage superimposed on the GEBCO (2003) bathymetric grid of the oceans. The positions of the sites studied in detail are indicated. Thin blue lines show the exclusive economic zone boundaries of the coastal states (taken from marineregions.org, shapefile v. 8)**

**Figure 2: Details of the bathymetry at the sampling sites along the Vema Fracture Zone/Transform showing the positions of the deployed gear. See also Table 1.**

**Table 1: Positions of sampling sites along the Vema transect and in the Puerto Rico Trough. Abbreviations: AUV = Autonomous Underwater Vehicle ABYSS (with internal dive number shown in parentheses); GC = Gravity Corer; MUC = Multicorer; Plank = Plankton Net; EBS = Epi-benthos sled, CTD = Conductivity-Temperature-Depth sensor on rosette water sampler; DS = Chain-bag dredge. # denotes stations where Miniature Autonomous Plume Recorders (MAPR, see Baker and Millburn, 1997), which detect turbidity and Eh variation in the water column, were attached to the wire above the deployed gear.**

| Site Number | Bounding box | Location/plate age* | Stations |
|---|---|---|---|
| **Vema Fracture Zone and Transform** | | |
| 2 | 10°44′N/25°06′W 10°41′N/25°03′W | Easternmost Vema/ 109 Ma | 1-1CTD, 2-1AUV (#160), 2-2GC#, 2-3MUC#, 2-4MUC, 2-5MUC, 2-6EBS, 2-7EBS, 3-1DS |
| 4 | 10°28′N/31°07′W 10°24′N/31°01′W | 81Ma(N), 63Ma(S) | 4-1AUV, 4-2Plank, 4-3MUC, 4-4MUC#, 4-5MUC, 4-6GC, 4-7AUV (#162), 4-8EBS, 4-9EBS, 4-10GC# |
| 5 | 10°22′N/32°13′W | 74Ma | 5-1DS |
| 6 | 10°23′N/36°58′W 10°20′N/36°55′W | North of FZ/43Ma | 6-1MUC, 6-2AUV (#163), 6-3MUC#, 6-4MUC#, 6-5MUC#, 6-6GC#, 6-7EBS, 6-8EBS |
| 7 | 10°13′N/36°32′W | 45Ma | 7-1DS |
| 8 | 10°45′N/42°43′W 10°42′N/42°39′W | Active Transform, ca. 10Ma. "Cannat"-Region | 8-2MUC, 8-3Plank, 8-4EBS, 8-5MUC#, 8-6MUC, 8-7MUC, 8-8CTD tow-yo#, 8-9GC#, 8-10MUC, 8-11MUC, 8-12GC# |
| 9 | 11°43′N/48°01′W 11°32′N/47°51′W | North of FZ/30Ma | 9-1AUV (#164), 9-2EBS, 9-3MUC#, 9-4MUC#, 9-5MUC, 9-6AUV (#165), 9-7GC#, 9-8EBS |
| 10 | 11°40′N/48°20′W | | 10-1DS |
| 11 | 12°06′N/50°31′W 12°04′N/50°26′W | South of FZ/62Ma | 11-1EBS, 11-2Plank, 11-3AUV (#166), 11-4EBS, 11-5MUC, 11-6MUC, 11-7MUC |
| **Puerto Rico Trough** | | |
| 12 | 19°51′N/66°59′W 19°46′N/66°45′W | Deepest basin adjacent to North | 12-1MUC#, 12-2MUC, 12-3MUC, 12-4GC, 12-5EBS, |

| | | Wall/ Age?? | 12-6EBS, 12-7MUC, 12-8MUC, 12-9Plank, 12-10GC |
|---|---|---|---|
| 13 | 19°51′N/67°10′W 19°43′N/66°58′W | Deepest basin adjacent to North Wall/ Age?? | 13-1MUC, 13-2MUC, 13-3MUC, 13-4EBS, 13-5EBS, 13-6GC |
| 14 | 19°05′N/67°11′W 19°00′N/67°07′W | South flank of Trough/ Age?? | 14-1EBS, 14-2EBS, 14-3MUC, 14-4MUC, 14-5MUC |

\* - plate age extracted from 6-minute-resolution age grids of Müller et al. (2008). In cases where the site lies within the Fracture Zone valley, plate ages to north (N) and south (S) are given.

### 3.1    Vema Fracture Zone and Transform

#### 3.1.1    Site 2

Site 2 lies north of the region defined as the Vema Fracture Zone, although in this region the "Fracture Zone" does not appear as a single linear crustal feature and is instead characterized by numerous blocks, bounded on their southern sides by short (<45 km long) WNW-ESE-trending escarpments which may be short fracture zone traces or pseudofaults marking the migration of overlapping spreading centres (Hey, 1977). Site 2 lies in a flat sedimented area between two such blocks and is on the oldest crust sampled during the transect. It lies within the Cretaceous Normal Superchron (Helsley & Steiner, 1969), a period from 120.6 to 83 Ma when the polarity of the magnetic field did not change, making an absolute age for the region difficult to assign. The age of 109Ma we have used (see Table 1) is based on an interpolation between identified older and younger anomalies assuming constant spreading rate (Müller et al., 2008). The sampled area lies to the north (sediment and biological sampling) and on the flank (dredge sampling) of a >16 km-wide massif which rises from the abyssal plain at 5500m to a minimum depth of 4650 m (see Figure 2). The massif shows some linear bathymetric ridges oriented NNW-SSE which resemble abyssal hill fabric, suggesting this massif is a piece of exposed oceanic crust. Dredge sampling at station 3-1DS yielded both sediment and highly altered pillow basalt samples with thick Mn-crusts.

The AUV-ABYSS was deployed in its multibeam configuration to produce a high-resolution bathymetric map of 5.5 km$^2$ (ca. 2.5x2.2 km) of the seafloor. The results, gridded at 1m, are shown in Figure 3

**Figure 3: The AUV-map of Site 2. For location of the mapped area, see Figure 2. Inset shows a perspective view of the mounds in the NW quadrant with a 2x vertical exaggeration (North shown by arrow).**

We identified several features of interest on this high-resolution map of deep, old crust. The map shows several sedimentary structures which appear to have been created by currents flowing westward. We identified asymmetric ripples (amplitude 30-80 cm, wavelength 20-30 m, steeper slope to the west, implying current from the east) and also scour structures around some prominent mounds (see Figure 3 inset). Note that this flow direction is in contrast to the regional deep-water currents which should flow from west to east (see Section 3.2 below) - this may be the result of the effects of local topography on the flow field (e.g., Turnewitsch et al., 2013). In the northern part of the surveyed area we

see a region of curved, E-W orientated striations, reminiscent of the furrows found in other deep sea regions and investigated, for example, by Flood (1983). A number of these striations are characterised by regularly spaced pits, sometimes elongated along the strike of the feature. These pits are less than a metre deep and range from 20-50 m in width.

The prominent mounds stand up to 25m above the base of the scour gullys which surround them and 20 m above the average surrounding seafloor - their geological nature is not discernible from mapping alone. Some possible explanations for these structures are that they are the tips of underlying crustal blocks or that they are features which have been constructed by precipitation from outflowing fluids - in either case they are evidently less affected by currents than the surrounding sediments.

### 3.1.2 Site 4

Site 4 lies within the Fracture Zone valley (Figure 2), adjacent to 81 Ma crust in the north and 63 Ma crust in the south. The area lies in 5800 m water depth, to the north and west the seafloor rises to a minimum depth of 5000m on bathymetric highs related to abyssal hill fabric. Sampling of one such high 120 km west of Site 4 (at station 5-1DS) returned Mn crusts, basaltic pillow lava fragments and gabbro (see below).

Approximately 6 km$^2$ of seafloor were mapped with the AUV using the 200 kHz multibeam sonar from a nominal altitude of 80m. The results are shown in Figure 4. The map shows the southern margin of a slumped sediment mass, presumably flowing off the massif to the north. Far more spectacular than the bathymetry is, however, the co-registered redox potential (Eh). Redox potential is often used in hydrothermal exploration to search for reducing chemical species (Fe2+, $H_2$, $H_2S$, $CH_4$) dissolved in the water column (e.g., Baker et al., 2016). During the bathymetric survey, the vehicle encountered one major and two minor Eh anomalies. In hydrothermal exploration an Eh response of >0.04 mV/s would be taken as a clear signal of hydrothermal activity (Baker et al., 2016) - the major anomaly registered at Site 4 has a maximum ΔEh of 0.18 mV/s. No bathymetric feature associated with this major anomaly is seen, although the region lies on the southwest margin of the surveyed area. We note however that the survey area is very close to the supposed trace of the Fracture Zone plane - no signs of any tectonic features on the seafloor were seen, however.

**Figure 4: Multibeam bathymetry with superimposed along-track redox potential (as delta Eh, in mV/s) from the AUV-survey at Site 4.**

### 3.1.3 Site 5

At Site 5 we performed one dredge haul on the northern slope of the Fracture Zone valley. The local bathymetry and the position of the dredge haul are shown in Figure 5. The dredged structure is flanked to the west by clear volcanic abyssal hill fabric and the rocks recovered suggest that the dredged massif has a typical magmatic crust construction, as altered pillow basalts, dolerites and one coarse gabbro block were recovered.

**Figure 5: The location of dredge haul 5-1DS.**

### 3.1.4 Site 6

Site 6 was located north of the fracture zone trace, on 43 Ma crust. The area studied is a flat sedimented region with water depths of around 5150 m. Both the AUV and the C-EBS returned photographs of the seafloor, the AUV also generated a side-scan sonar map, shown in Figure 6. The seafloor has a very homogeneous acoustic reflectivity over most of the area, with only the eastern margin of the survey area showing some small blocks on the seafloor. Pictures taken by the C-EBS while resting on the seafloor prior to sampling show a generally flat, sedimented seafloor with small mounds surrounded by a ring of *Sargassum*, apparently similar to the features seen at Site 9 (see Section 3.1.7 below)

**Figure 6: Side-scan sonar image of the seafloor at Site 6 from AUV dive 6-2AUV.**

**Figure 7: Images from the video (top) and still (bottom) camera attached to the C-EBS deployed at Site 6.**

### 3.1.5 Site 7

Site 7 also was only sampled with a dredge haul. The regional bathymetry is shown in Figure 8. The axis-parallel abyssal hill fabric is evident everywhere. The samples collected were all pillow basalt fragments, some with signs of fresh preserved glass. This is consistent with the much smaller slope dredged here (250 m (from 5000 m to 4750 m)) compared to that sampled at Site 5 (1200 m, from 5600 m to 4400 m) permitting access to only the upper (pillow lava) parts of the oceanic crust.

**Figure 8: The bathymetry around dredge station 7-1DS.**

### 3.1.6 Site 8

Site 8 was situated on the youngest crust sampled during the cruise, at ca. 10 Ma in the active transform fault valley. This site is ca. 120 km from the spreading axis which lies to the north of the transform and ca. 180 km from the spreading axis to the south. The water depth is very constant at 5180m - this probably represents the effects of sedimentation and repeated shaking by earthquakes, levelling the seafloor. Bad weather meant that we were not able to deploy the AUV, but all other station work could be completed. Figure 2 shows the location of all gear deployments. The area is located close to the southern wall of the transform valley in an area that had been previously mapped and sampled (Cannat et al., 1991; Cipriani et al., 2009).

We performed a CTD tow-yo (continuous heaving and lowering of the instrument while the vessel is slowly steaming) at Site 8 (8-8CTD tow-yo) with one Miniature Autonomous Plume Recorder (MAPR) including an oxidation-reduction potential (ORP) sensor (Walker et al., 2007) attached to the carousel water sampler and a second one to the cable 30m above the CTD. In the last part of the tow-yo section, the ORP sensor mounted directly on the CTD showed a small decrease in Eh (Figure 9). Even though the signal is below the threshold used in Baker et al. (2016) for the absolute decrease of Eh at a mid-ocean ridge hydrothermal site (2mV), we are confident that the observed reduction is due to

hydrothermal activity because a decrease in Eh was observed in two consecutive heaving-lowering sequences over several data points.

As the signal was only observed by the ORP sensor attached to the CTD and not by the sensor 30m above, the source can be concluded to have both low flow rate and low temperature. However, this is one of very few places where, up to now, hydrothermal emissions have been detected in the off-axis region and extends the distance over which off-axis activity occurs hugely - the previous "record-holders" were the Lost City site (15 km off-axis, Kelley et al., 2005) and the Drachenschlund vent (>9 km off-axis, Melchert et al., 2008)

**Figure 9: Top: ΔEh from 1 minute low pass filtered data during a tow-yo station in the transform valley. Smaller dots denote downcasts during the tow-yo, bigger dots the upcasts. The position of the CTD was determined using a Posidonia ultra-short-baseline navigation transponder. Bottom: time-series of measured Eh values. A small drop at approximately 7:10pm followed by a larger drop at approximately 7:30pm, corresponding to the strongest ΔEh signal in the top panel, can be clearly seen.**

Evidence for active upward movement of water was also seen in the sediment core (8-12GC) collected close to the 8-8CTD tow-yo track (for location, see Figure 2). A plot of total alkalinity vs. depth for all sediment cores collected during the cruise is shown in Figure 10. At most of the stations, total alkalinity values increase only slightly with sediment depth. This is typical for deep-sea sediments, which receive low amounts of degradable organic carbon, resulting in low mineralization intensities. The gravity corer 8-12GC shows a distinctly different profile. Total alkalinity increases up to 12 meq/L, indicating enhanced mineralization processes at this site. Since increased organic matter input can be ruled out as a potential source of this input, seepage of upward-flowing fluids carrying a signature of geochemical processes occurring at greater sediment depth and/or higher temperatures offers a likely explanation for this observation. In the MUC profiles at the same site no higher total alkalinity was observed.

**Figure 10: Total alkalinity vs. depth in core for all gravity corer deployments. Note the increasing alkalinity with depth in core 8-12GC.**

3.1.7   Site 9

Site 9 lies to the west of the spreading axis and is on the north side of the Fracture Zone, on 30 Ma crust. The regional seafloor fabric is characterized by abyssal hill ridges oriented approximately 020° (Figure 11). The AUV was deployed in an area of relatively flat sediment immediately to the east of one of these abyssal ridges and produced a bathymetric map of a 10 km$^2$ (2x5 km) region (dive 9-1AUV, see Figure 12). The vehicle attempted to maintain an altitude of 80 m during this mapping (actual altitude range 78-85 m). Even at this altitude, one distinct Eh anomaly in the water column was seen. There appears to be no clear feature on the seafloor which might be associated with this anomaly. A sub-region of the mapped area was then the subject of a photo survey (dive 9-6AUV, see Figure 12). The photos showed a thoroughly sedimented seafloor (no outcrop seen in any of the pictures) with ubiquitous signs of both biological activity and *Sargassum* falls. Typical photographs are shown in Figure 13. We see scattered pieces of *Sargassum* debris, generally associated with small mounds or pockmarked areas on the seafloor (whether

these mounds accumulate *Sargassum* because they act as barriers to *Sargassum* drift in tidal currents or the *Sargassum* is actively dragged there by the fauna is unclear).

**Figure 11: The location of the unsuccessful dredge station 10-1DS (yellow) relative to the Site 9 deployments. The area surveyed by the AUV (data shown in Figure 8) is marked by the green box. All three MUC deployments at Site 9 were so close together as to fall within the size of the orange symbol on the map.**

**Figure 12: Microbathymetry of the seafloor at Site 9 from the 9-1AUV dive. The along-track rate of change in Eh (mV/s) measured aboard the vehicle during the mapping is also shown. The yellow-shaded area shows the region of the photo survey for dive 9-6AUV. For the broader bathymetric setting of this dive area, see Figure 11.**

**Figure 13: Two seafloor images from Site 9. Approximate size of each image is 8x8 m. In almost all images taken during dive 9-6AUV, signs of burrowing, grazing, pockmarks and mounds are seen. Many pictures also contain pieces of *Sargassum* debris.**

The first EBS deployment at Site 9 (9-2EBS, for location see Figure 11) accidentally occurred in a field of Mn-nodules. Pictures of the seafloor taken by the EBS-mounted camera are shown in Figure 14,

**Figure 14: Pictures of Mn-nodules (A, B) and *Sargassum* debris partially buried by sediment (D) on the seafloor along the track of 9-2EBS (for location, see Figure 11). Picture C shows two of the Mn-nodules (cut, left and uncut, right) recovered in the EBS net. Photos A,B, D © N. Brenke, photo C © T. Walter.**

### 3.1.8   Site 10

Site 10 was only occupied for an unsuccessful dredge station. The location of this station, and its position relative to Site 9, is shown in Figure 11. From the bathymetry in this region, it is unclear whether the ridge which we attempted to sample is a portion of uplifted lithosphere on the southern side of the Fracture Zone (similar to that described near the ridge axis by Bonatti et al., 2005) or the southern margin of the northern side of the Fracture Zone. If the former is the case then the unsuccessful deployment is perhaps not surprising - we attempted to dredge a thickly sedimented seafloor rather than a fault scarp on an uplifted block!

### 3.1.9   Site 11

Site 11 is the most westerly Site occupied in the Vema Fracture Zone and, although it lies south of the projected trace of the main Vema Fracture Zone, it shows clear fracture zone-parallel structures. A map of the gear deployment locations is shown in Figure 15. A series of NW-SE terraces in the bathymetry are clearly visible running through the deployment area. These terraces are also visible in the side-scan sonar images produced during 11-3AUV dive, see Figure 16.

**Figure 15: The ship-based bathymetry around Site 11. The area covered by the 11-3AUV camera and side-scan sonar survey is shown as a box.**

**Figure 16: 11-3AUV side-scan sonar map of Site 11. Note that the true geographical position of the side-scan mosaic was determined by matching the prominent NW-SE terraces to lineations visible in the ship-based bathymetric maps. This correction (534 m towards 310° with respect to to the dead-reckoning position calculated by the AUV) was confirmed by the Posidonia position of the C-EBS tracks, both of which are visible in the side-scan record.**

The side-scan results from dive 11-3AUV show the area to be geologically complex. The terraces form a series of lineaments in the southern half of the mapped area. Both north and south of these lineaments are clearly defined areas characterized by elongated pits - the pit region south of the lineaments appears to be related to a prominent, 3m-high break in slope with deeper bathymetry to the south. No clear bathymetric signature is associated with the more northern pit regions. It appears that the clear acoustic signature of the pits on the sidescan record results from the very low vehicle altitude (10m) used for the acquisition - the shallow grazing angle greatly enhances even small topographic effects.

The photographs taken by the AUV during dive 11-3AUV suggest the seafloor is geologically active. Lineations marked by white colouration and sediment blocks are regularly seen (see, for example, image 11-3AUV_IM002716, Figure 17). In some cases the sediment is seen to be indurated and fractured (image 11-3AUV_IM007954, Figure 17). During the dive, the track of the C-EBS was also crossed - this provides both an absolute scale for the photographs as well as giving an indication of the seafloor disturbance the sledge produces (Figure 17).

**Figure 17: Images taken during 11-3AUV with labelled features. The width of the C-EBS is 1.8 m, providing a direct scale for picture 11-3AUV_IM002448 and an approximate scale for the other images assuming approximately constant vehicle height above ground during the survey.**

### 3.2    Hydrography of the Vema Fracture Zone

An important component of the deep sea habitat is the water masses and their movements above the seafloor. They have relevance both for nutrient supply (trace metals, oxygen) as well as larval dispersal (near-bottom currents). The Vema Fracture Zone is an important conduit through the Mid-Atlantic Ridge for cold and dense bottom water flowing from the western to the eastern Atlantic basin. For the water with potential temperatures below 2°C, an eastward transport through the Vema fracture zone of 2.1-2.3Sv was estimated by McCartney et al. (1991) and a similar transport of 2.1-2.4Sv below a level of no motion at 3640 m was observed by Fischer et al. (1996). The depth of the level of no motion roughly coincides with the depth at which the fracture zone widens significantly. At the surface, the North Equatorial Current (NEC), with a wind-induced westward flow that forms the southern part of the subtropical gyre, is found (e.g., Bourles et al., 1999).

**Figure 18: Top: locations of the vertical profiles of temperature and salinity. AUV measurements are shown as circles, the station where measurements were carried out with a CTD attached to a water sampler is shown by a star. Bottom: potential temperature -salinity diagram at the stations.**

During the cruise 8 vertical profiles of temperature and salinity at 6 different sites were obtained (Figure 18). Seven of these were measured by the AUV and one during a tow-yo station in the transform valley where a Sea-Bird Electronics, Inc. SBE9plus system was attached to a carousel water sampler. Data from the descent leg of the AUV dives and the first downcast of the water sampler at each site are shown in the panels of Figure 18.

In a temperature-salinity diagram of all stations (Figure 18) the different water masses dominating the deep flow in the Vema Fracture Zone can be clearly distinguished. The densest is the Antarctic bottom water (AABW, θ<2°C: Zenk and Morozov, 2007) with slightly lower salinities compared to the warmer North Atlantic deep water (NADW) and the freshest and warmest Antarctic

Intermediate Water (AAIW). Towards the east the NADW gets increasingly fresher. Data from the World Ocean Circulation Experiment (WOCE) sections A05 (24°N) and A06 (7.5°N) show that this freshening is accompanied by a decrease in oxygen content (see http://www.ewoce.org and Schlitzer, 2000). While at the western boundary the NADW contains higher oxygen concentrations (up to 270 µmol/kg at A06) than the AABW (240 µmol/kg at A06), its concentration decreases towards the African coast to values similar to the concentration in the AABW (http://www.ewoce.org and Schlitzer, 2000).

In vertical profiles of (potential) temperature and salinity (Figure 19) the influence of AABW at the seafloor is seen to decrease eastward, with both temperature and salinity increasing significantly (from approximately 1.8° to 2.3° and from approximately 34.82 to 34.86 respectively). The strongest change in bottom water mass characteristics occurs between the transform fault (Site 8) and the first station in the eastern basin (Site 6). A decrease in the thickness of the AABW layer towards the interior of the western basin is observed because in this region the AABW flows northward along the western flank of the Mid-Atlantic Ridge.

**Figure 19: Vertical profiles below 3500m of potential temperature (left), absolute temperature and salinity at the stations shown in Figure 18**

### 3.3 Puerto Rico Trough

Due to the extreme depths in the Puerto Rico Trough, 6000 m-rated equipment with pressure vessels (for camera, electronics etc.) such as the epi-benthic sledge or the AUV could not be deployed. Our knowledge of the seafloor habitat is therefore limited to information from the ship-mounted multibeam sonar and the multicorer-samples.

**Figure 20: Bathymetry of the Puerto Rico Trough. Also shown are the locations of Sites 12-14.**

The multibeam sonar shows the deepest part of the trough to be located at the foot of the steep E-W trending north wall (the regional bathymetry of the Puerto Rico Trough is given, for example, by ten Brink, 2005). The seafloor in this area is extremely flat, with total variations in relief of <200 m (between 8400 - 8200 m) over a distance of >100 km. Sites 12 and 13 were located in this deep region. The Puerto Rico Trough shallows towards the south as the island of Puerto Rico is approached and the terrain becomes rougher. Site 14 was located on this terrain.

### 3.4 Sediment Grain Size

Sediment grain-size analysis shows that the silt-clay fraction dominates at all sites (Figure 21). The very deep sites (12, 13) located in the Puerto Rico trench (~8000 m) show up to 98 % of silt-clay, while the 5000 m site (14) in the trench (closer to the island of Puerto Rico) showed a high proportion of the coarser-grained sediment fractions. Fine, medium, and coarse sand contributed from 8-12 % of the total sediment composition in the Vema Fracture Zone sites. Sites located east of the MAR (2, 4, 6) show lower contents of fine, medium, and coarse sand (0–7 %) when compared to those west of the MAR (9, 11). We see no systematic vertical variations in grain-size distribution over the 5 cm sampling distance.

**Figure 21: Relative sediment grain size contribution (%) at each site for the sediment layers (0-1, 1-2, 2-3, 3-4, and 4-5 cm). Each bar shows the contribution of each sediment fraction and their respective standard deviations.**

## 4   Conclusions

The Vema-TRANSIT cruise provided some startling discoveries and confirmed other previous results. We were able to demonstrate the presence of active hydrothermal flow in the transform fault region, leading to an order of magnitude increase in the maximum distance off-axis that such flow has been found (from previously 15 to now >120 km off-axis). Most near-bottom AUV deployments, covering crustal ages from ca. 110 Ma to 0 Ma, returned evidence for a geologically active seafloor - from Eh-anomalies in the water column up to 80 m above the seafloor, suggesting active release of reduced compounds, to sediment fracturing, with some fractures marked by white discolorations. All studied sites which lay within the fracture zone valley showed such features, some sites situated outside the valley also showed indications of geological activity. At all sites where seafloor photographs were taken, we found extensive evidence of biological activity, the more easterly sites also showed ubiquitous signs of *Sargassum* accumulation on the seafloor.

### References

Baker, E.T., Millburn, H.B., 1997. MAPR: A new instrument for hydrothermal plume mapping. Ridge Events 8, 23-25.

Baker, E.T., Resing, J., Haymon, R.M., Tunnicliffe, V., Lavelle, J.W., Martinez, F., Ferrini, V.L., Walker, S.L., Nakamura, K., 2016. How many vent fields? New estimates of vent field populations on ocean ridges from precise mapping of hydrothermal discharge locations. Earth Planet. Sci. Lett. 449, 186-196.

Barnett, P.R.O., Watson, J., Connelly, D., 1984. A Multiple Corer for Taking Virtually Undisturbed Samples From Shelf, Bathyal and Abyssal Sediments. Oceanologica Acta 7, 399-408.

Bergman, E.A., Solomon, S.C., 1992. On the strength of Oceanic Fracture Zones and Their Influence on the Intraplate Stress Field. J. Geophy. Res. 97, 365 - 377.

Bonatti, E., Brunelli, D., Buck, W.R., Cipriani, A., Fabretti, P., Ferrante, V., Gasperini, L., Ligi, M., 2005. Flexural uplift of a lithospheric slab near the Vema transform (Central Atlantic): Timing and mechanisms. Earth Planet. Sci. Lett. 240, 642-655.

Bourles, B., Molinari, R.L., Johns, E., Wilson, W.D., Leaman, K.D., 1999. Upper layer currents in the western tropical North Atlantic (1989-1991). Journal Of Geophysical Research-Solid Earth And Planets 104, 1361-1375.
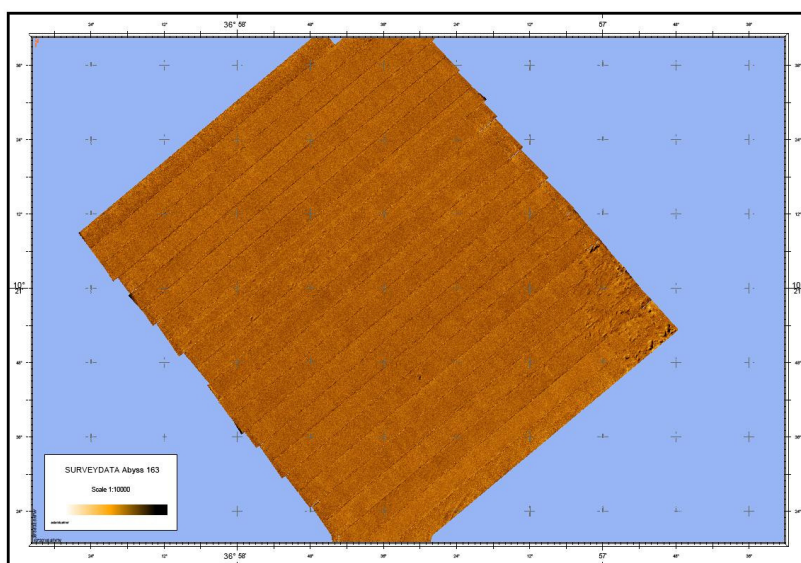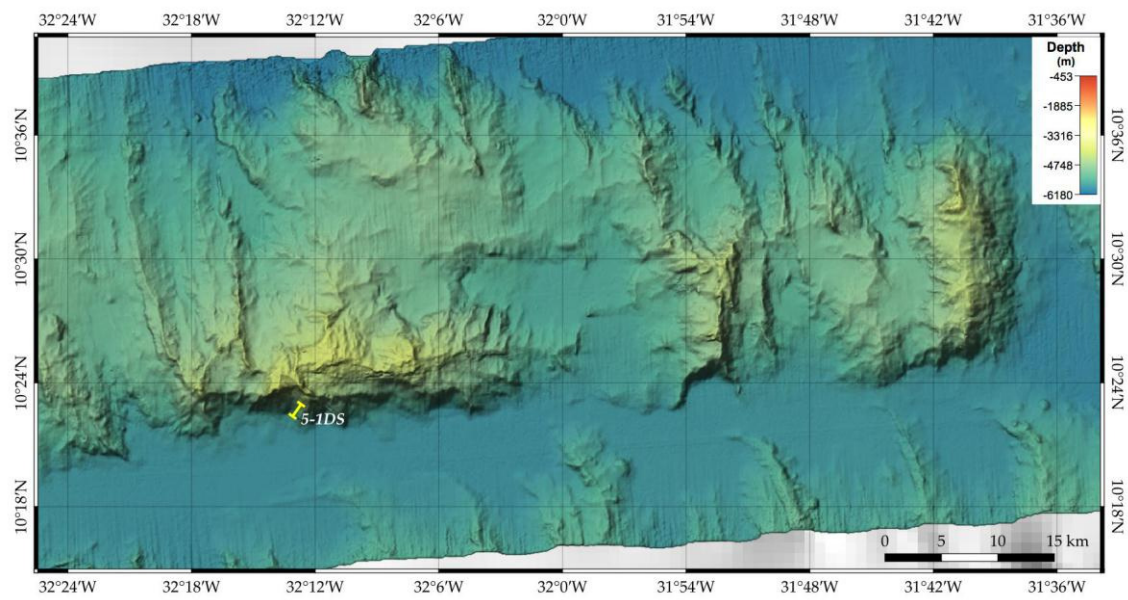
Brandt, A., Elsner, N., Brenke, N., Golovan, O., Malyutina, M.V., Riehl, T., Schwabe, E., Wuerzberg, L., 2013. Epifauna of the Sea of Japan collected via a new epibenthic sledge equipped with camera and environmental sensor systems. Deep-Sea Research Part Ii-Topical Studies In Oceanography 86-87, p43-55.

Brown, L., 2010. A new technique for depicting terrain relief, NACIS 2010 - North American Cartographic Information Society, St Petersburg, Florida, USA, p. 16.

Cannat, M., Mamaloukasfrangoulis, V., Auzende, J.M., Bideau, D., Bonatti, E., Honnorez, J., Lagabrielle, Y., Malavieille, J., Mevel, C., 1991. A Geological Cross-Section of the Vema Fracture-Zone Transverse Ridge, Atlantic-Ocean. Journal Of Geodynamics 13, 97-117.

Cannat, M., Seyler, M., 1995. Transform tectonics, metamorphic plagioclase and amphibolitization in ultramafic rocks of the Vema transform fault (Atlantic Ocean). Earth And Planetary Science Letters 133, 283-298.

Caress, D.W., Chayes, D.N., 1996. Improved processing of Hydrosweep DS multibeam data on the R/V Maurice Ewing. Marine Geophysical Researches 18, 631-650.

Cipriani, A., Bonatti, E., Brunelli, D., Ligi, M., 2009. 26 million years of mantle upwelling below a segment of the Mid Atlantic Ridge: The Vema Lithospheric Section revisited. Earth And Planetary Science Letters 285, 87-95.

Clement, L., Thurnherr, A.M., St Laurent, L.C., 2017. Turbulent Mixing in a Deep Fracture Zone on the Mid-Atlantic Ridge. Journal of Physical Oceanography 47, 1873-1896.

Detrick, R.S., Cormier, M.H., Prince, R.A., Forsyth, D.W., Ambos, E.L., 1982. Seismic constraints on the crustal structure within the Vema Fracture Zone. Journal Of Geophysical Research-Solid Earth 87, 10599.

Duin, E., Mesdag, C.S., Kok, P., 1984. Faulting in Madeira Abyssal-Plain Sediments. Marine Geology 56, 299-308.

Dzierma, Y., Thorwart, M., Rabbel, W., Siegmund, C., Comte, D., Bataille, K., Iglesia, P., Prezzi, C., 2012. Seismicity near the slip maximum of the 1960 Mw 9.5 Valdivia earthquake (Chile): Plate interface lock and reactivation of the subducted Valdivia Fracture Zone. Journal Of Geophysical Research-Solid Earth 117, 6312.

Ferron, B., Mercier, H., Speer, K., Gargett, A., Polzin, K., 1998. Mixing in the Romanche Fracture Zone, J Phys Oceanogr, pp. 1929-1945.

Fischer, J., Rhein, M., Schott, F., Stramma, L., 1996. Deep water masses and transports in the Vema Fracture Zone. Deep Sea Research Part I: Oceanographic Research Papers 43, 1067-1074.

Flood, R.D., 1983. Classification of Sedimentary Furrows and a Model for Furrow Initiation and Evolution. Geological Society of America Bulletin 94, 630-639.

Hensen, C., Scholz, F., Nuzzo, M., Valadares, V., Gràcia, E., Terrinha, P., Liebetrau, V., Kaul, N., Silva, S., Martínez-Loriente, S., Bartolome, R., Piñero, E., Magalhães, V.H., Schmidt, M., Weise, S.M., Cunha, M., Hilario, A., Perea, H., Rovelli, L., Lackschewitz, K., 2015. Strike-slip faults mediate the rise of crustal-derived fluids and mud volcanism in the deep sea. Geology 43, 339-342.

Hey, R., 1977. A new class of "pseudofaults" and their bearing on plate tectonics: A propagating rift model. Earth Planet . Sci. Letts. 37, 321-325.

Kelley, D.S., Karson, J., Früh-Green, G.L., Yoerger, D.R., Shank, T.S., Butterfield, D.A., Hayes, J.M., Schrenk, M.O., Olson, E.J., Proskurowski, G., Jakuba, M., Bradley, M., Larson, B., Ludwig, K., Glickson, D., Buckman, K., Bradley, A.S., Brazelton, W.J., Roe, K., Elend, M.J., Delacour, A., Bernasconi, S.M., Lilley, M.D., Baross, J.A., Summons, R.E., Sylva, S.P., 2005. A serpentinite-hosted ecosystem: The Lost City hydothermal field. Science 307, 1428-1434.

Lagabrielle, Y., Mamaloukas-Frangoulis, V., Cannat, M., Auzende, J.M., Honnorez, J., Mevel, C., Bonatti, E., 1992. Vema Fracture Zone (Central Atlantic): Tectonic and Magmatic Evolution of the Median Ridge and the Eastern Ridge-Transform Intersection Domain. J. Geophy. Research 97, 331 - 351.

Lange, D., Tilmann, F., Rietbrock, A., Collings, R., Natawidjaja, D.H., Suwargadi, B.W., Barton, P., Henstock, T., Ryberg, T., 2010. The Fine Structure of the Subducted Investigator Fracture Zone in Western Sumatra as Seen by Local Seismicity. Earth and Planetary Science Letters 298, 47-56.

Ledwell, J.R., Montgomery, E.T., Polzin, K.L., St Laurent, L.C., Schmitt, R.W., Toole, J.M., 2000. Evidence for enhanced mixing over rough topography in the abyssal ocean, Nature, pp. 179-182.

Macdonald, K.C., Fox, P.J., 1983. Overlapping spreading centres: new accretion geometry on the East Pacific Rise. Nature 302, 55-58.

Mamaloukasfrangoulis, V., Auzende, J.M., Bideau, D., Bonatti, E., Cannat, M., Honnorez, J., Lagabrielle, Y., MALAVIEILLE, J., Mevel, C., Needham, H.D., 1991. Insitu Study of the Eastern Ridge Transform Intersection of the Vema Fracture-Zone. Tectonophysics 190, 55-71.

Mammerickx, J., 1970. Morphology of Aleutian Abyssal Plain. Geological Society of America Bulletin 81, 3457-+.

Matthews, K.J., Muller, R.D., Wessel, P., Whittaker, J.M., 2011. The tectonic fabric of the ocean basins. Journal Of Geophysical Research 116, 12109.

McCartney, M.S., Bennett, S.L., Woodgate-Jones, M.E., 1991. Eastward Flow Through the Mid-Atlantic Ridge at 11-Degrees-N and Its Influence on the Abyss of the Eastern Basin. Journal of Physical Oceanography 21, 1089-1121.

McGuire, J.J., Beroza, G.C., 2012. A Rogue Earthquake Off Sumatra. Science 336, 1118-1119.

Melchert, B., Devey, C.W., German, C.R., Lackschewitz, K.S., Seifert, R., Walter, M., Mertens, C., Yoerger, D.R., Baker, E.T., Paulick, H., Nakamura, K., 2008. First evidence for high-temperature off-axis venting of deep crustal/mantle heat: The Nibelungen hydrothermal field, southern Mid-Atlantic Ridge. Earth Planet. Sci. Lett. 275, 61-69.

Minshull, T.A., Dean, S.M., Whitmarsh, R.B., 2014. The peridotite ridge province in the southern Iberia Abyssal Plain: Seismic constraints revisited. Journal Of Geophysical Research-Solid Earth 119, 1580-1598.

Muller, R.D., Roest, W.R., 1992. Fracture zones in the North Atlantic from combined Geosat and Seasat data. Journal Of Geophysical Research 97, 3337-3350.

Müller, R.D., Sdrolias, M., Gaina, C., Roest, W.R., 2008. Age, spreading rates, and spreading asymmetry of the world's ocean crust. Geochem. Geophys. Geosyst. 9, Q04006.
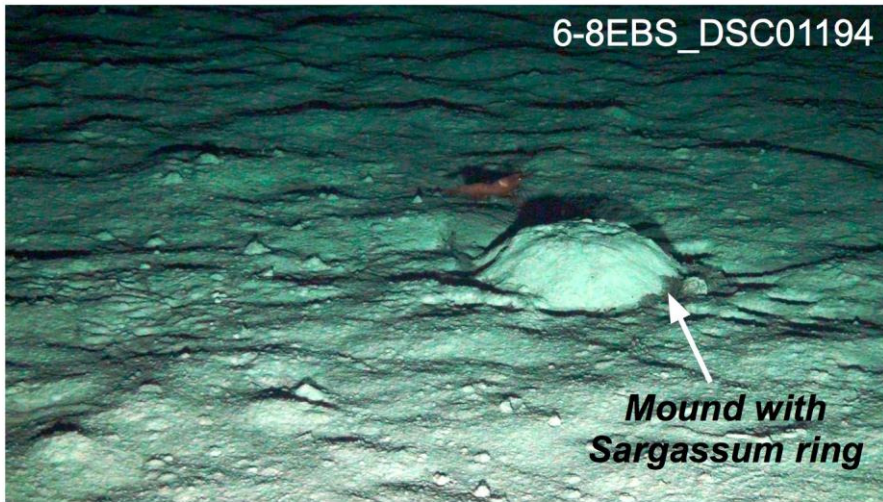
Mullineaux, L.S., Speer, K.G., Thurnherr, A.M., Maltrud, M.E., Vangriesheim, A., 2002. Implications of cross-axis flow for larval dispersal along mid-ocean ridges. Cahiers De Biologie Marine 43, 281-284.

Nakajima, J., Hasegawa, A., 2006. Anomalous low-velocity zone and linear alignment of seismicity along it in the subducted Pacific slab beneath Kanto, Japan: Reactivation of subducted fracture zone? Geophysical Research Letters 33.

Polzin, K.L., Speer, K.G., Toole, J.M., Schmitt, R.W., 1996. Intense mixing of Antarctic Bottom Water in the equatorial Atlantic Ocean, Nature, pp. 54-57.

Polzin, K.L., Toole, J.M., Schmitt, R.W., 1997. Spatial variability of turbulent mixing in the abyssal ocean. Science 276, 93-96.

Potts, C.G., White, R.S., Louden, K.E., 1986. Crustal Structure of Atlantic Fracture-Zones .2. the Vema Fracture-Zone and Transverse Ridge. Geophysical Journal of the Royal Astronomical Society 86, 491-&amp;.

Pratt, R.M., 1965. Ocean-Bottom Topography - Divide Between Sohm and Hatteras Abyssal Plains. Science 148, 1598-&amp;.

Prince, R.A., Forsyth, D.W., 1988. Horizontal extent of anomalously thin crust near the Vema Fracture Zone from the three-dimensional analysis of gravity anomalies. Journal Of Geophysical Research-Solid Earth 93, 8051-8063.

Schlitzer, R., 2000. Electronic atlas of WOCE hydrographic and tracer data now available. Eos 81, 45.

Scholz, F., Hensen, C., Reitz, A., Romer, R.L., Liebetrau, V., Meixner, A., Weise, S.M., Haeckel, M., 2009. Isotopic evidence (87Sr/86Sr, δ7Li) for alteration of the oceanic crust at deep-rooted mud volcanoes in the Gulf of Cadiz, NE Atlantic Ocean. Geochimica Et Cosmochimica Acta 73, 5444-5459.

ten Brink, U., 2005. Vertical motions of the Puerto Rico Trench and Puerto Rico and their cause. J Geophys Res-Sol Ea 110, B06404.

Thurnherr, A.M., St Laurent, L.C., Speer, K.G., Toole, J.M., Ledwell, J.R., 2005. Mixing associated with sills in a canyon on the midocean ridge flank, J Phys Oceanogr, pp. 1370-1381.

Tucholke, B.E., Schouten, H., 1989. Kane Fracture-Zone. Marine Geophysical Researches 10, 1-39.

Turnewitsch, R., Falahat, S., Nycander, J., Dale, A., Scott, R.B., Furnival, D., 2013. Deep-sea fluid and sediment dynamics-Influence of hill- to seamount-scale seafloor topography. Earth-Science Reviews 127, 203-241.

van Andel, T.H., Von Herzen, R.P., Phillips, J.D., 1971. The Vema fracture zone and the tectonics of transverse shear zones in oceanic crustal plates. Marine Geophysical Researches 1, 261-283.

Walker, S.L., Baker, E.T., Resing, J., Nakamura, K., McLain, P.D., 2007. A new tool for detecting hydrothermal plumes: an ORP Sensor for the PMEL MAPR, AGU Fall Meeting Abstract V21D-0753, San Fransicso.

Wilson, J.T., 1965. A New Class of Faults and Their Bearing on Continental Drift. Nature 207, 343-&amp;.

Zenk, W., Morozov, E., 2007. Decadal warming of the coldest Antarctic Bottom Water flow through the Vema Channel. Geophysical Research Letters 34.
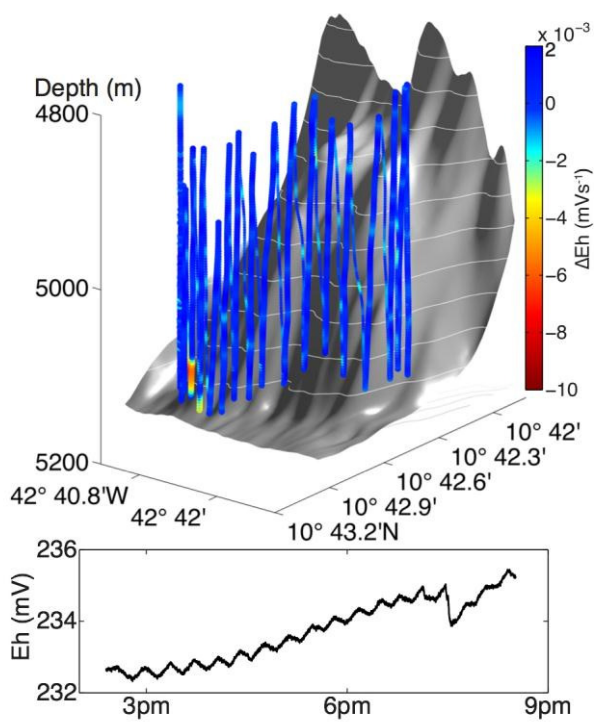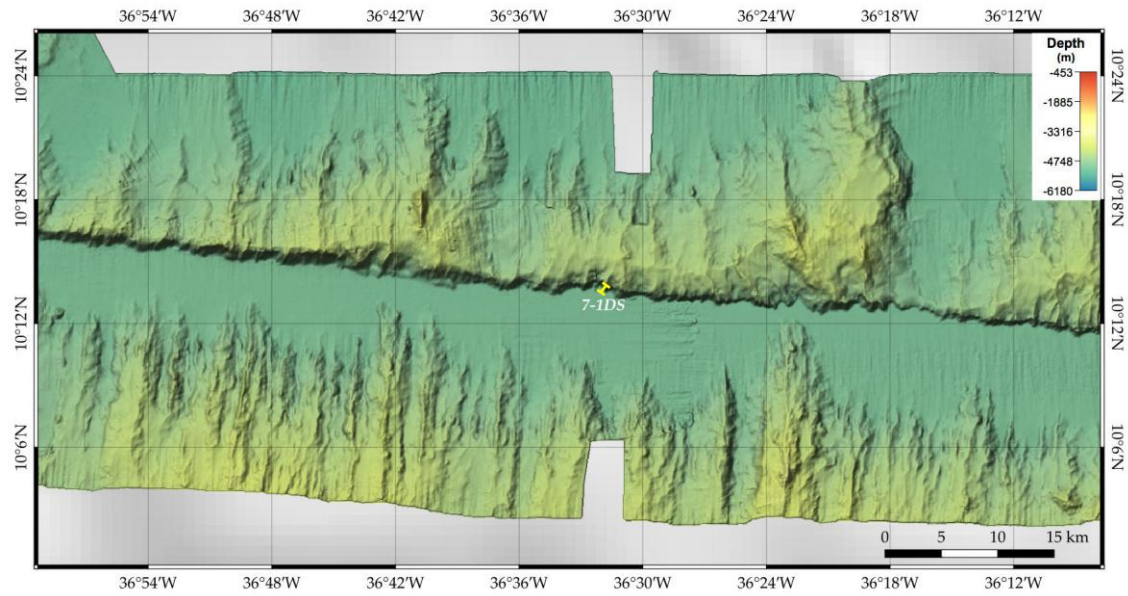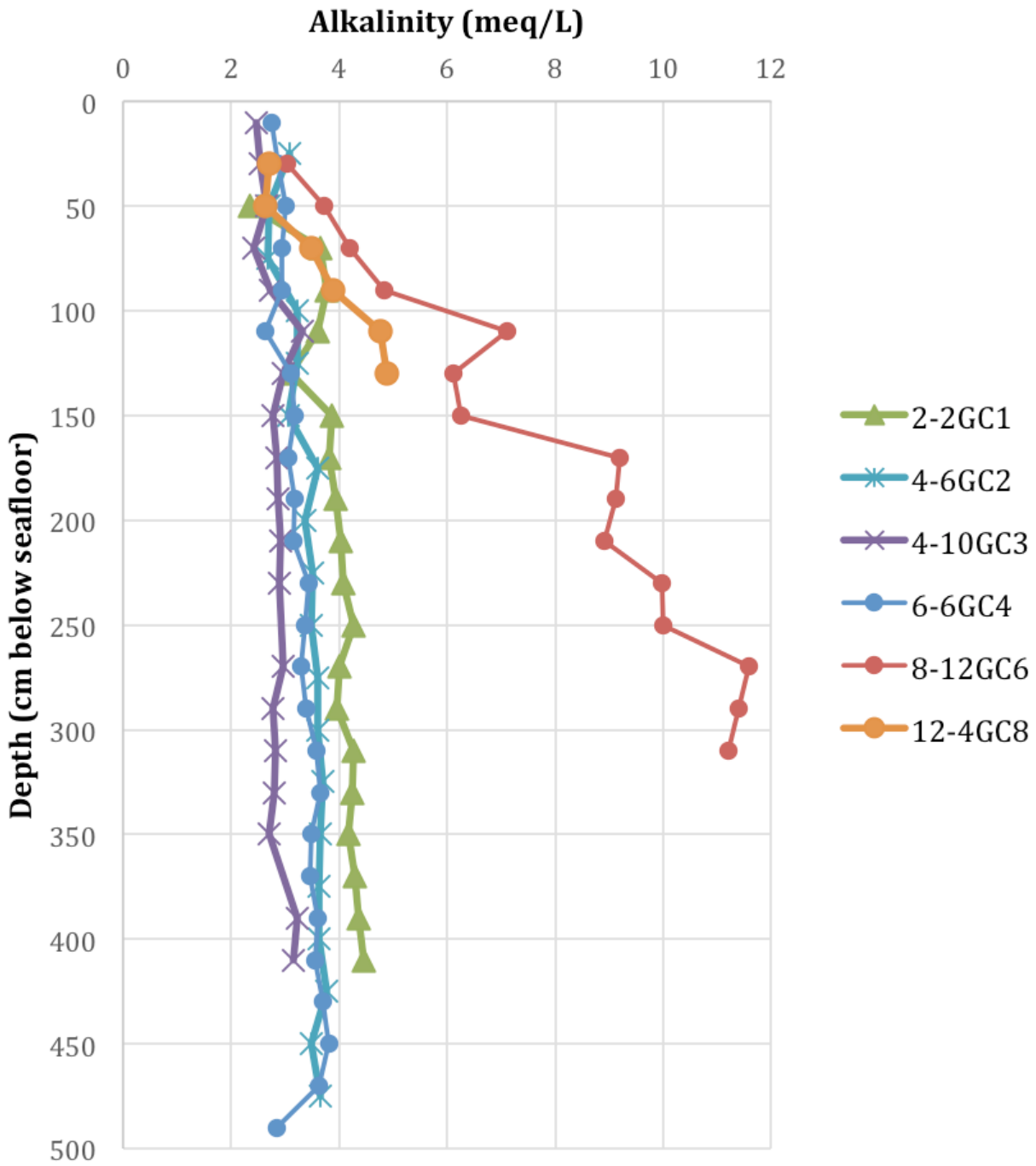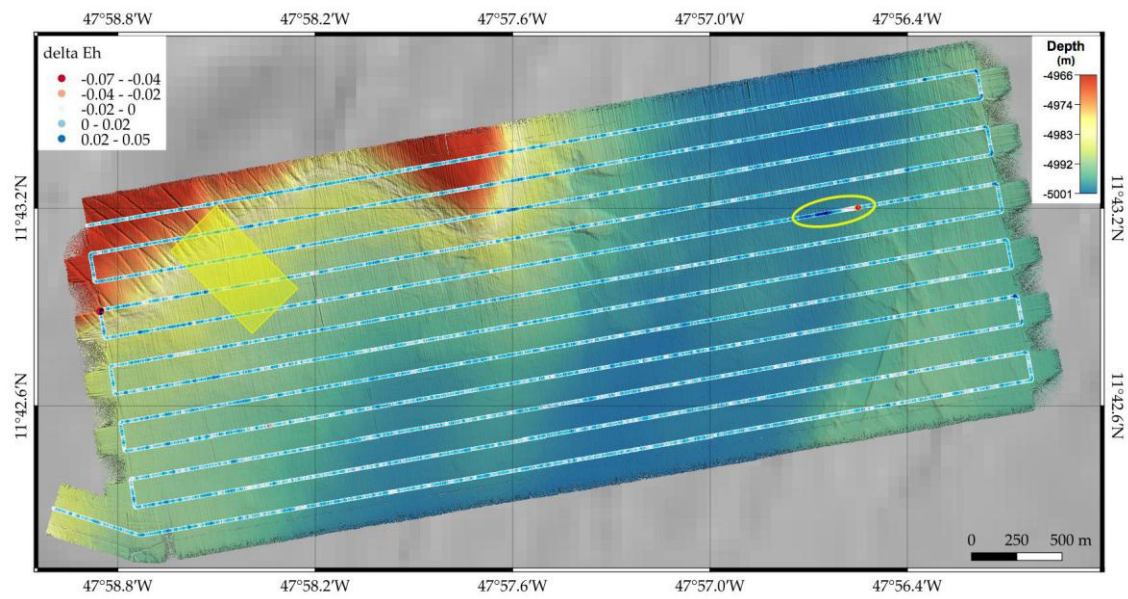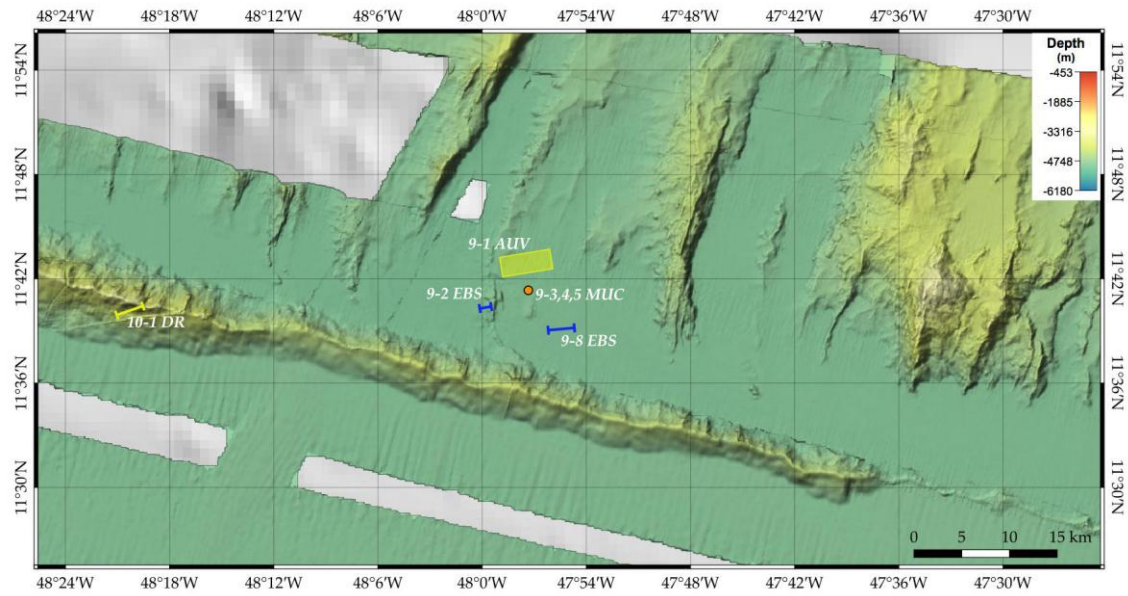
# Seafloor images from Site 6

6-8EBS_DSC01194
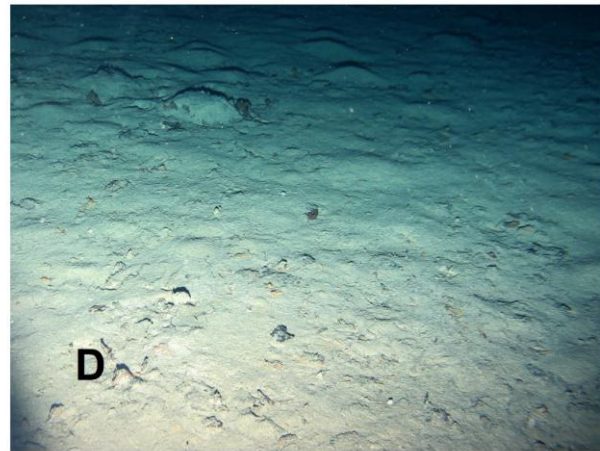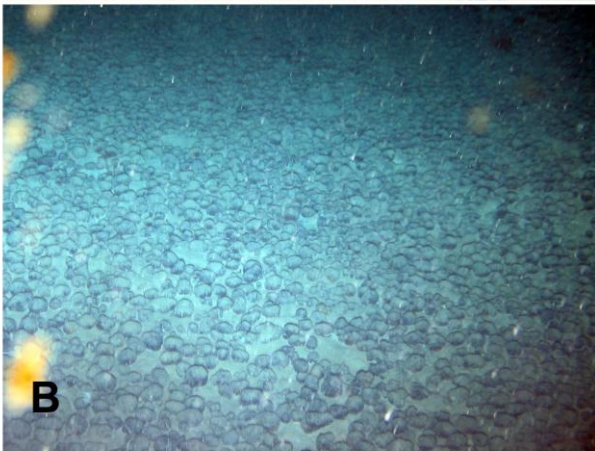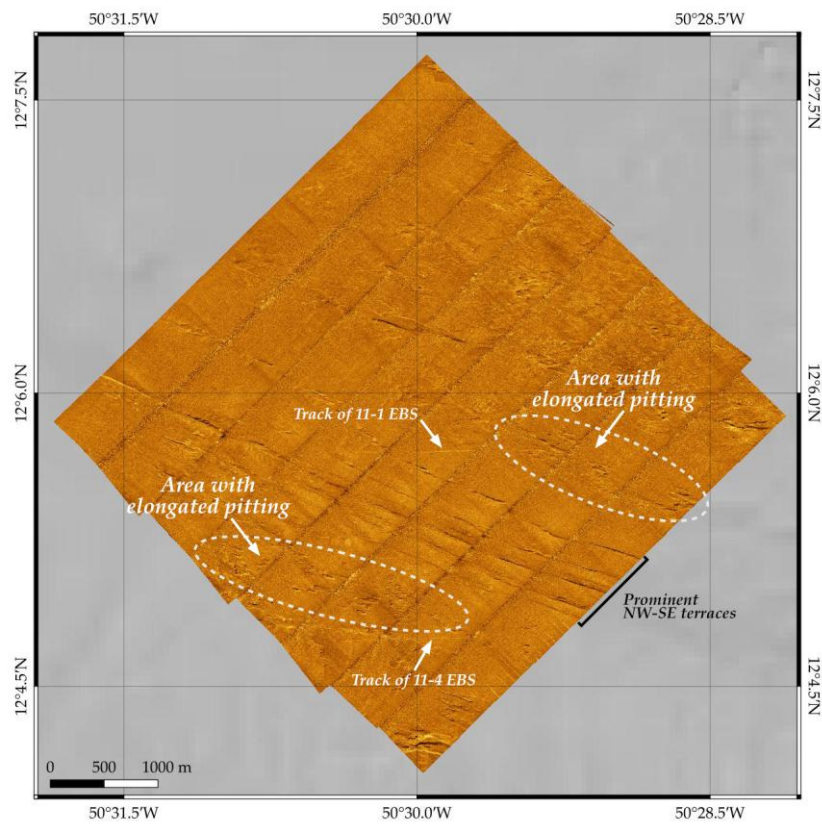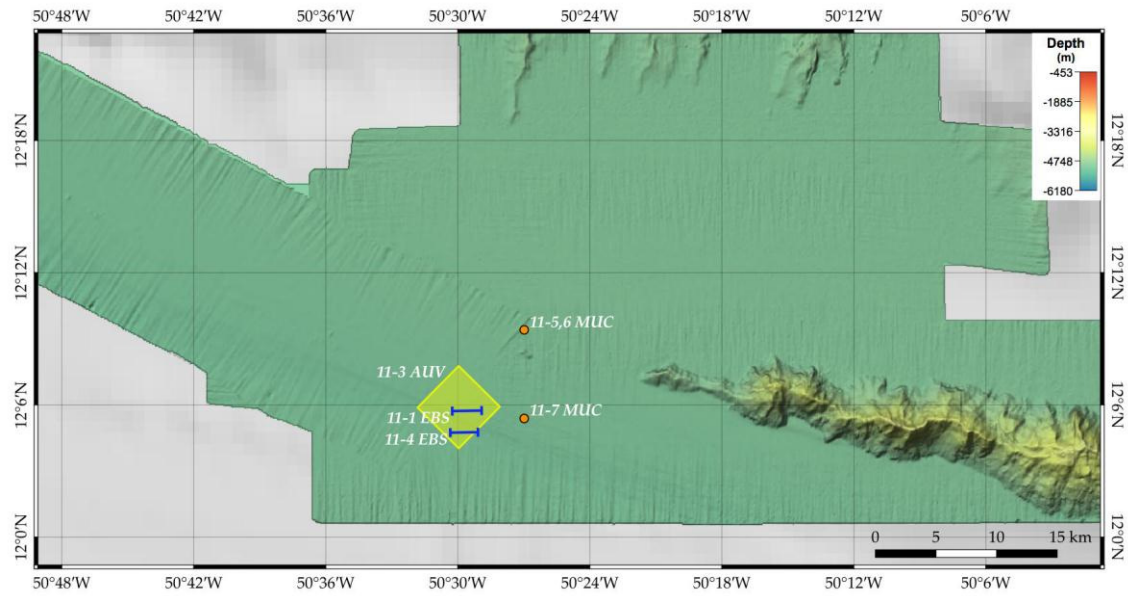
*Mound with Sargassum ring*

6-8EBS_IMG-0600

**Typical seafloor images from Site 9**



Mound with surrounding sargassum debris

Mound with pock-marks and surrounding sargassum debris

9-6AUV_IM005794

Grazing track

Bright pockmarks

Stellate markings around ?burrows

9-6AUV_IM005756

## 9-2EBS



A

B

C

D

# Typical seafloor images from Site 11



11-3AUV_IM002716

Fracture with white coloration

Mounds with pockmarks

11-3AUV_IM007954

Sediment fracturing and uplift

11-3AUV_IM002448

Mound with pockmarks

Trace of 11-1EBS